Theoretical Studies on the Hydrolysis Mechanism of N-(2-oxo-1,2-dihydro-pyrimidinyl) Formamide

Yong Wu,[†] Ying Xue,*[,†,‡] Dai Qian Xie,*[,§] Chan Kyung Kim,[||] and Guo Sen Yan[†]

College of Chemistry, Key Lab of Green Chemistry and Technology, Sichuan University, Chengdu 610064, People's Republic of China, State Key Laboratory of Biotherapy, West China Hospital, Sichuan University, Chengdu 610041, People's Republic of China, Institute of Theoretical and Computational Chemistry, Key Laboratory of Mesoscopic Chemistry, School of Chemistry and Chemical Engineering, Nanjing University, Nanjing 210093, People's Republic of China, and Department of Chemistry, Inha University, Inchon 402-751, Korea

Received: July 17, 2006; In Final Form: January 6, 2007

Density functional theory (B3LYP) and ab initio (MP2) methods with the 6-31G(d,p) basis set are used to study the mechanisms for the hydrolysis of N-(2-oxo-1,2-dihydro-pyrimidinyl) formamide (PFA) in the gas phase. The direct and the water-assisted hydrolysis processes are considered, involving one and two water molecules, respectively. Three different pathways are explored in each case. In the first pathway, the O atom of water first attacks at the C atom of amide while one H atom of water transfers toward the oxygen of amide, leading to an intermediate of tetrahedral coordinated carbon with two OH groups. In the subsequent step, the hydroxyl H atom transfers to the N atom of pyrimidine ring and the C−N covalent bond of amide dissociates simultaneously. In the second path, the O and one H of water attack at the C of amide and the N of pyrimidine ring, respectively, while the C−N bond of amide dissociates. In the third path, three processes occur simultaneously: the O of water attacks at the C of amide, one H atom attacks at the N of amide, and the C−N bond of amide is broken. It is shown that the second pathway is favored for the direct hydrolysis while the first pathway is favored for the water-assisted hydrolysis. It is also shown that the water-assisted hydrolysis is slightly more favorable than the direct hydrolysis. Moreover, solvent effects on five pathways are evaluated with Monte Carlo simulation (MC) and free energy perturbation methods. It is shown that the solvent water slightly reduces the energy barrier in each pathway. The first pathway in the water-assisted hydrolysis remains the most favorable when the solvent effects of bulk water are taken into account.

1. Introduction

Cytosine, one of the four fundamental bases constituting the double helix of DNA, exists naturally in all nucleic acids. It can interact via hydrogen bonds with the other nucleic acid bases, mainly with guanine. To understand the complex biological system, many researches concerning cytosine were comprehensively conducted in the past decades.[1−11] In particular, various modified nucleosides and nucleotides with cytosine as base, occurring naturally or synthesized artificially, received a great deal of attention due to their mutagenic, antimutagenic, antiviral, and antitumor activities.[12−14] Recently, Anastasi et al. synthesized the potent nonclassical nucleoside antiviral drugs: formamidine-3TC (3TC = 2′,3′-dideoxy-3′-thiacytidine) analogues.[15] They found experimentally that the replacing of formamidine side chains at the 4-N position of cytosine base could enhance the lipophilicity and bioavailability of the parent drug 3TC. On the other hand, the formamidine group also served as the protector of the amino group in the base. When the amidine side chains were hydrolyzed step by step to the corresponding amino group, as shown in Scheme 1, the formamidine-3TC exhibited the antiviral activity as a drug. Moreover, the different substituents on the formamidine may affect its stability to hydrolysis. Anastasi guessed that those hydrolytic reactions could involve in a common 4-N-formyl intermediate (see Scheme 1).[15] However, the detailed mechanism of the formamidine-3TC hydrolysis has not yet been subject of any experimental and theoretical investigations.

SCHEME 1: Schematic Pathway to Generate 3TC

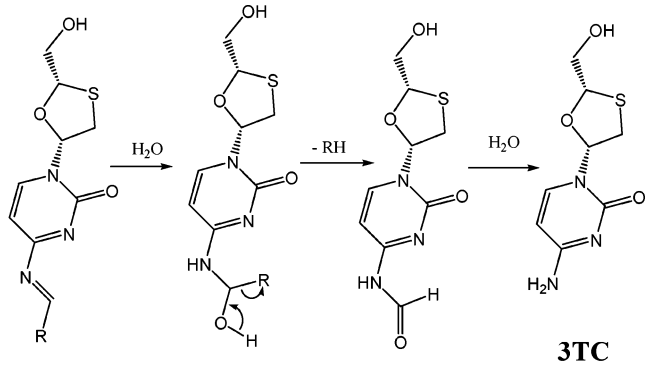

R= -N(CH$_3$)$_2$, -N(C$_4$H$_8$O), -(C$_6$H$_5$)$_2$, or -N(*p*-Y-C$_6$H$_5$)$_2$, (Y=OMe, F, CH$_3$, COOEt)

Therefore, within this scenario, it would be valuable to study the key step of the complex reaction process, the hydrolysis of the common intermediate formamide-3TC. For the simple formamide $HCONH_2$, its hydrolysis mechanism has been computationally investigated.[16,17] Mitzner et al.[16] explored the mechanism of formamide hydrolysis using density functional

* Corresponding authors. E-mails: xueyingscu@163.com (Y.X.), dqxie@nju.edu.cn (D.Q.X.).
[†] Key Lab of Green Chemistry and Technology, Sichuan University.
[‡] West China Hospital, Sichuan University.
[§] Nanjing University.
[||] Inha University.

10.1021/jp064510c CCC: $37.00 © 2007 American Chemical Society
Published on Web 02/13/2007

SCHEME 2: Possible Hydrolysis Pathways of PFA (*k, m, p* = 0, 1)

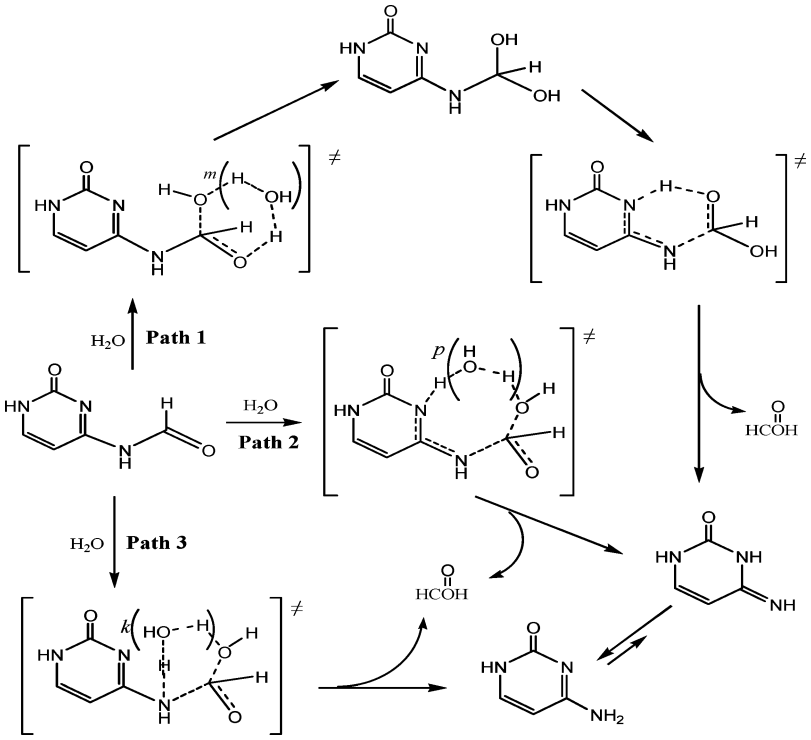

theory (DFT) and cluster-continuum method and found that two pathways, stepwise and concerted processes, were very competitive with the very closed energy barriers of about 50 kcal/mol. Carloni and his co-workers[17] have also studied the hydrolysis process of formamide by use of ab initio molecular dynamic simulations and obtained that the energy barrier was about 45 kcal/mol. In our system, the large group connecting to the N atom of the formamid must influence the mechanism of formamide hydrolysis. Considering that the ribose ring of 3TC is far from the hydrolysis reaction center, we selected a simple model compound, N-(2-oxo-1, 2-dihydro- pyrimidinyl) formamide (PFA), to mimic the formamide-3TC through the replacement of the sugar ring of the cytidine nucleoside by an H atom. Thus, the research object here became to the reaction mechanism of the hydrolysis of the title compound.

In the present study, three possible pathways for the hydrolysis of PFA are considered on the basis of the known information about cytosine isomerization and formamide hydrolysis (Scheme 2). In each case, two processes, the direct hydrolysis (with one water molecule) and the water-assisted hydrolysis (with two water molecules), were considered. For the gas-phase reactions, the hybrid density functional theory (B3LYP) and the second-order Møller-Plesset (MP2) perturbation theory have been used in our calculations. It is well-known that solvent effects play an important role in determining transition states, rates of reaction, equilibrium constants, and the other quantities of chemical and biochemical processes. In our previous work, we adopted the quantum chemical molecular orbital method and Monte Carlo (MC) simulation with free energy perturbation (FEP) technique to study effects of solvents on the aza-Wittig reaction of iminophosphoranes and the isomerization of imidazolines.[18−21] In this study, the potential energy profiles of the direct and water-assisted hydrolysis processes of the compound PFA in the gas phase and in water were obtained. The effect of water as solvent was studied using the Monte Carlo free energy perturbation method.

2. Computational Details

2.1. Gas-Phase Calculation. In the gas phase, the geometric structures of the reactant complexes, intermediates, transition states, and product complexes were optimized at the B3LYP/6-31G(d,p)[22,23] and MP2/6-31G(d,p)[24−28] levels of theory. The stationary points were confirmed by the harmonic frequency analysis as a minimum with all positive frequencies or as a transition state with only one imaginary frequency. At the B3LYP/6-31G(d,p) level, the intrinsic reaction coordinate (IRC)[29] calculations were performed to verify the transition states. In this way, the geometries along the minimum energy path (MEP) were also given. For all points along MEP, atomic charges were obtained via the CHELPG procedure[30] at the B3LYP/6-31G(d,p) level. All calculations were carried out by using Gaussian 03 program.[31]

2.2. Monte Carlo Simulation. To examine the solvent effects on the PFA hydrolysis reaction, the changes of the free energies of solvation were determined using Monte Carlo simulation with free energy perturbation method (MC-FEP). In the present model, a pre-equilibrated box containing 400 solvent water molecules was used for each free energy perturbation simulation. Simulations were carried out in the isothermic-isobaric ensemble (NPT; 1atm, 298.15K) using Metropolis sampling and periodic boundary conditions. The solvent−solvent nonbonded cutoff (RCUT) was set to 12.0 Å, and the solute−solvent nonbonded cutoff (SCUT) was also set to 12.0 Å. Preferential sampling was employed with the WKC parameter set to 300. Perturbations were carried out with use of double-wide sampling scheme.[32] The geometries of solute were mutated along the simulation, which were obtained in IRC calculations at the B3LYP/6-31G(d,p) level in the gas phase. No sampling of the internal degrees of freedom was performed. Parameters determining volume changes and solute rotations and translations were adjusted to have an acceptance level ca. 40%. The system was perturbed between adjacent structural points i and j, and the free energy

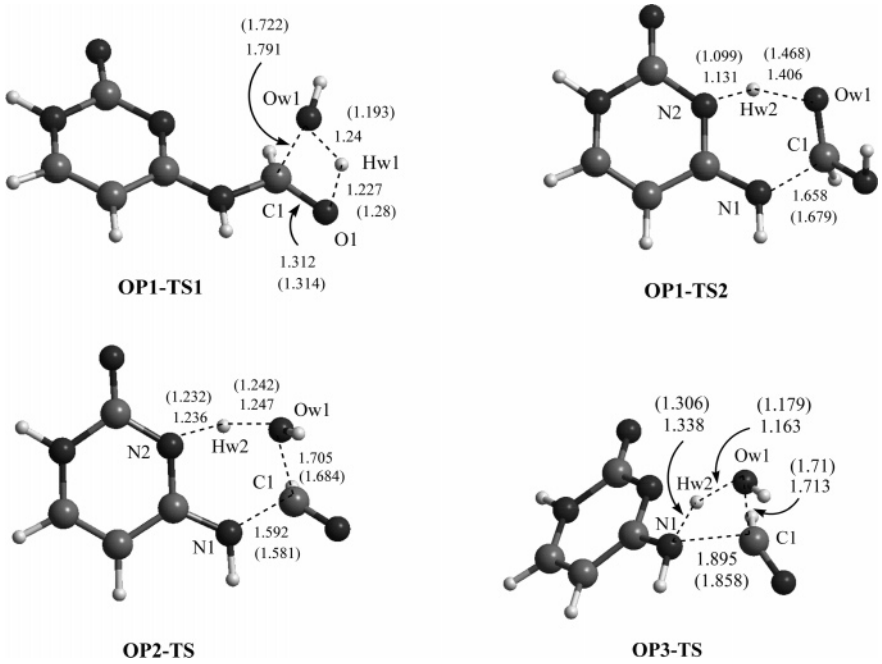

Figure 1. Optimized TS geometries (OP1−TS1, OP1−TS2, OP2−TS, and OP3−TS) for the direct hydrolysis of PFA at the B3LYP/6-31G(d,p) level of theory (MP2/6-31G**, in parentheses; bond length, in Å).

differences ΔG_{ij} were calculated via Zwanzig perturbation expression[33] as follows:

$$\Delta G_{ij} = G_j - G_i = -kT \ln\{\exp[-(E_j - E_i)/kT]\}_i \quad (1)$$

where E_i is the total energy of the point i, k is the Boltzman constant, and T is the absolute temperature. Each simulation involved 10^6 configurations of equilibration and 2×10^6 configurations of averaging. All of the simulations were executed using the BOSS program.[34]

As shown below, the intermolecular interaction is described by a potential energy function consisting of Coulomb and Lennard-Jones (LJ) terms between the atom i in the molecule a and atom j in the molecule b, which are separated by a distance r_{ij}

$$\Delta E_{ab} = \Sigma\Sigma(q_i q_j e^2/r_{ij} + 4\epsilon_{ij}[(\sigma_{ij}/r_{ij})^{12} - (\sigma_{ij}/r_{ij})^6]) \quad (2)$$

The four-site TIP4P model[35−37] was used for the solvent water. For the solute, the CHELPG charges were calculated for each system at the B3LYP/6-31G(d,p) level in the gas phase and were assigned to all atoms in the solute as partial charges; Lennard-Jones parameters for solutes were taken from the OPLS all-atom force field[38] in BOSS program database and scaled linearly in going from their reactant to product values. The crossing terms were obtained using the geometric combining rules:

$$\epsilon_{ij} = (\epsilon_i \epsilon_j)^{1/2}, \sigma_{ij} = (\sigma_i \sigma_j)^{1/2} \quad (3)$$

In this study, 390 and 389 water molecules in an approximate $20 \times 20 \times 30$ Å^3 box were used for the direct and water-assisted PFA hydrolysis reactions, respectively.

3. Results and Discussions

In our work, as illustrated in Scheme 2, six reaction pathways of the direct hydrolysis and the water-assisted hydrolysis were investigated. In order to conveniently state the hydrolysis mechanism in this article, three paths of the direct hydrolysis were denoted as A-path 1, A-path 2, and A-path 3, while three processes of the water-assisted hydrolysis were named as B-path 1, B-path 2, and B-path 3, respectively. In path 1, the oxygen of water first attacks at the C atom of amide while one H atom of water transfers toward the O atom of amide, leading to an intermediate of tetrahedral coordinated carbon with two OH groups. Then the hydroxyl H atom transfers to the nitrogen of pyrimidine ring and the C−N bond of amide dissociates simultaneously. In path 2, the O and one H of water attack at the C of amide and the N of pyrimidine ring, respectively, while the C−N bond of amide dissociates. In path 3, three processes occur simultaneously: the O atom of water attacks at the C of amide, one H atom transfers to the N of amide, and the C−N bond of amide is broken. Therefore, Path 1 is stepwise, while Path 2 and Path 3 are concerted in the hydrolysis reaction of PFA.

3.1. Stationary Point Structures and Energetics in the Gas Phase. *3.1.1. Direct Hydrolysis Reaction of PFA.* On the potential energy surfaces (PES) of the direct hydrolysis reaction of PFA, four different transition states were located and their optimized structures are depicted in Figure 1. The optimized Cartesian coordinates and geometrical structures of all stationary points along the PES are shown in Supporting Information Part 1 and Part 2, respectively.

A-Path 1. As shown in Figure s1 of Supporting Information Part 2, the geometries of complexes OP1−CM1 and OP1−CM2, transition states OP1−TS1 and OP1−TS2, and the intermediate OP1−IM were optimized at the B3LYP/6-31G** level. In OP1−CM1, one can see that Hw1 and Ow1 atoms of water interact with O1 and H1 atoms of PFA to form hydrogen bonds, respectively. The distances of H1−Ow1 and O1−Hw1 are 2.6211 and 1.9753 Å, respectively. It is implied that the H1−Ow1 hydrogen bond is weaker than the O1−Hw1 hydrogen bond. Therefore, the complex OP1−CM1 mainly relies on the formation of the O1−Hw1 hydrogen bond in the reaction. In OP1−TS1, a four-membered ring structure, the distances of C1−Ow1, Hw1−Ow1, and Hw1−O1 are 1.7941, 1.2396, and 1.2272 Å, respectively. The distance of C1−N1 in OP1−TS1 is 1.3849 Å, which is 0.005 Å longer than that in OP1−CM1.

The imaginary frequency of 1682.71i cm^{-1} is mainly associated with the vibrational mode in which the Hw1 atom transfers from Ow1 to O1 atom. IRC results indicate that two processes occur simultaneously in this reaction step: the Ow1 atom attacks at the C1 atom and the Hw1 atom transfers toward the O1 atom. After the reaction surmounts the transition state OP1−TS1, the intermediate OP1−IM can be generated. Intermediate OP1−IM has a tetrahedral coordinated carbon with two OH groups. The length of C1−N1 bond is 1.4875 Å, which is 0.1077 and 0.1026 Å longer than that in OP1−CM1 and OP1−TS1, respectively. This indicates that the C1−N1 bond in OP1−IM is weaker than that in OP1−CM1 and OP1−TS1 due to that the hybridization of C1 atom changes from sp^2 in OP1−CM1 to sp^3 in OP1−IM. In this process ongoing from OP1−CM1 to OP1−IM, the C1═O1 double bond changes to C1−O1 single bond and the n−π conjugation between N1 atom and C1═O1 double bond is eliminated, resulting in weakening and elongating of the C1−N1 bond. In addition, the distance of Hw2−N2 is 1.8941 Å in OP1−IM. Taking into account the tautomerization of cytosine, the Hw2 atom, we guess, maybe transfer from Ow1 to N2 atoms in the next reaction step. Under our hypothesis, the transition state OP1−TS2 was located in this pathway. In OP1−TS2, the distances of Hw2−N2, Hw2−Ow1, and C1−N1 are 1.1310, 1.4056, and 1.6786 Å, respectively. The imaginary frequency is 516.71i cm^{-1}, which is associated with the coupling of transfer of Hw2 and C1−N1 bond stretching mode. After the reaction overcomes the transition state OP1−TS2, the complex OP1−CM2 is produced. In OP1−CM2, the distances of Hw2−Ow1 and H1−N1 are 1.9400 and 2.3088 Å, respectively.

A-Path 2. As presented in Figure s2 of Supporting Information Part 2, the geometries of complexes OP2−CM1 and OP2−CM2 and the transition state OP2−TS were also optimized at the B3LYP/6-31G** level. It is important to note that, although the atom numbering of water is same in different reaction pathways, the atom maybe not the same in different reaction pathways. In OP2−CM1, the distances of Hw2−N2 and Ow1−H1 are 2.0854 and 2.1875 Å, respectively, indicating that the complex OP2−CM is formed with the hydrogen bond. The OP2−TS is a six-membered ring transition state. As shown in Figure 1, the distances of Hw2−N2, Hw2−O1, Ow1−C1, and C1−N1 are 1.2364, 1.2470, 1.7052, and 1.5918 Å, respectively. It is found that the six-membered ring is almost in a plane and that the Ow1 and C1 atoms deviate from the plane about 10° in the opposite direction. The imaginary frequency is 896.41i $cm^{-1}$and its vibrational mode is mainly associated with the coupling of the transfer of Hw2 atom from Ow1 to N2 atoms and the addition of Ow1 to C1 atoms, leading to the cleavage of C1−N1 bond. It is also found that the C2═N2 double bond is weakening as the C2−N1 single bond is enhancing in the transition state OP2−TS. Therefore, A-path 2 is a concerted process in the title reaction. In OP2−CM2, the distance of Ow1−Hw2 and H1−N1 are 2.0270 and 2.3798 Å, respectively. Note that the tautomerization of cytosine was not studied in our work because this process was very clear.

A-Path 3. As illustrated in Figure s3 of Supporting Information Part 2, the geometries of complexes OP3−CM1 and OP3−CM2 and the transition state OP3−TS were also optimized at the B3LYP/6-31G** level. In OP3−CM1, the distances of H1−Ow1 and Hw1−Ow1 are 2.6139 and 1.9761 Å, respectively, which are very close to those in OP1−CM1. One can see that the structure of OP3−CM1 is very similar to that of OP1−CM1 except the H atom position in water. Due to the Cs symmetry of PFA, OP3−CM1 and OP1−CM1 have the mirror-like relation. OP3−TS is also a four-membered ring transition state. The distances of Hw2−N1, Hw2−Ow1, Ow1−O1, and C1−N1 are 1.3378, 1.1628, 1.7130, and 1.8954 Å, respectively. It is found that the dihedral angle N1−C2−N1−C1 is −43.95°, indicating that the C1 atom is deviated from the plane of pyrimidine ring. The imaginary frequency is 1212.13i cm^{-1}. IRC results confirmed that this pathway is associated with the transfer of Hw2 atom from Ow1 to N1 atoms and the formation of the Ow1−C1 bond, leading to the cleavage of the C1−N1 bond. In OP3−CM2, the distances of H1−N2 and Hw2−Ow1 are 2.3782 and 1.0968 Å.

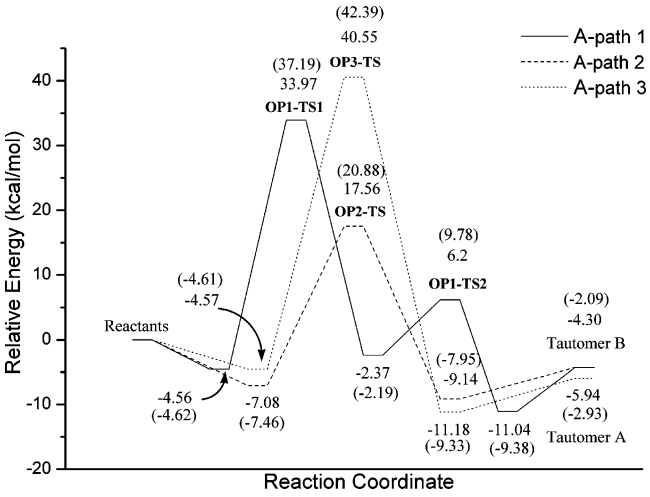

Figure 2. Energies profiles in direct hydrolysis of PFA.

TABLE 1: Relative Energies, Free Energies, and Solvation Energies to Reactant Complex in Direct Hydrolysis of PFA (in kcal/mol)

	B3LYP/ 6-31G(d,p)		MP2/6-31G (d,p)		Monte Carlo
	ΔE(gas)	ΔG(gas)	ΔE(gas)	ΔG(gas)	$\Delta(\Delta G$(sol))
			A-path 1		
OP1−CM1	0.0	0.0	0.0	0.0	0.0
OP1−TS1	38.53	41.61	41.81	45.29	−0.69
OP1−IM	2.19	5.61	2.43	6.13	3.92
OP1−TS2	10.76	14.38	14.4	18.26	2.19
OP1−CM2	−6.48	−6.0	−4.76	−4.43	10.2
			A-path 2		
OP2−CM1	0.0	0.0	0.0	0.0	0.0
OP2−TS	24.64	27.66	28.34	31.89	−4.29
OP2−CM2	−2.06	−2.83	−0.49	−1.14	3.83
			A-path 3		
OP3−CM1	0.0	0.0	0.0	0.0	0.0
OP3−TS	45.12	47.84	47.0	50.01	−2.01
OP3−CM2	−6.61	−8.02	−4.72	−4.94	−0.66

In addition, those stationary points on the PES of the direct hydrolysis reaction were reoptimized at the MP2/6-31G(d,p) level. The corresponding structure parameters are also presented in Figure 1 as well as Figures s1, s2, and s3 in Supporting Information Part 2. It is found that the geometries located at the MP2/ 6-31G(d,p) level are very close to those located at the B3LYP/6-31G** level.

The electronic energy and free energy profiles for the three pathways in the direct hydrolysis reaction in the gas phase were depicted in Figure 2 and Figure s4 of Supporting Information Part 2, respectively. Additional energy data, including the zero-point vibrational energy and thermal corrections are summarized in Table 1. From Figure 2 and Table 1, one can see that A-path 2 is more favorable than other pathways. For A-path 2, the energy barrier is 24.64 kcal/mol at the B3LYP/ 6-31G** level in vacuum, while it increases to 28.34 kcal/mol at the MP2/6-

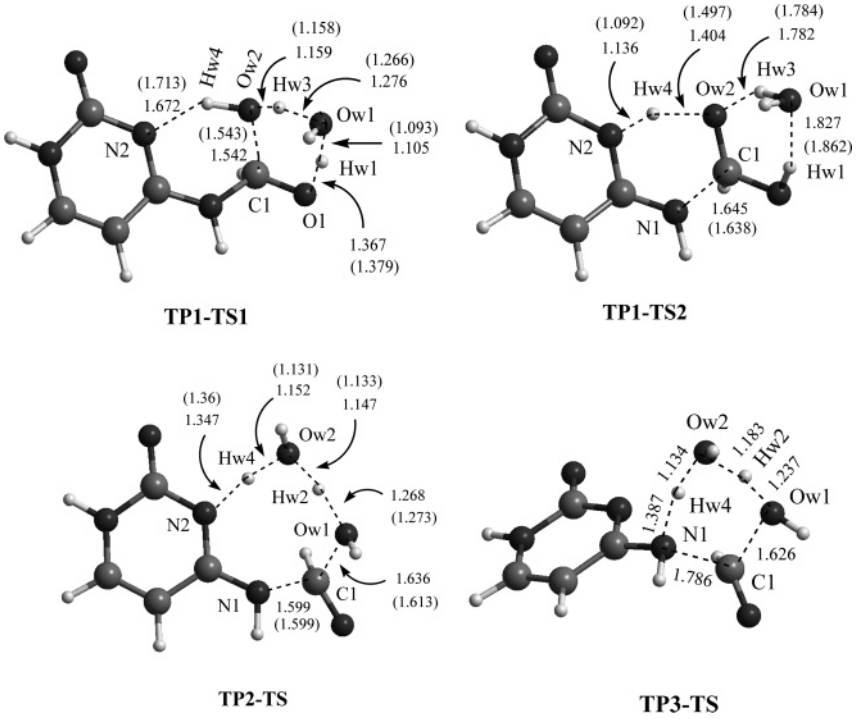

Figure 3. Optimized TS geometries (TP1−TS1, TP1−TS2, TP2−TS, and TP3−TS) for the water-assisted hydrolysis of PFA at the B3LYP/6-31G(d,p) level of theory (MP2/6-31G**, in parentheses; bond length, in Å).

31G** level in vacuum. For A-path 1, one can see that the rate-limiting step is the first one to surmount the transition state OP1−TS1. The energy barriers are 38.53 kcal/mol at the B3LYP/6-31G(d,p) level and 41.81 kcal/mol at the MP2/6-31G-(d,p) level, respectively. For A-path 3, the energy barrier is 45.12 kcal/mol in vacuum at the B3LYP/6-31G** level and 47.0 kcal/mol at MP2/6-31G(d,p) level, respectively. Therefore, for the reaction processes in the direct hydrolysis, our calculations figure out that the energy barriers calculated at the MP2/6-31G(d,p) level are about 2∼4 kcal/mol higher than those calculated at the B3LYP/6-31G(d,p) level. In Figure s4 of Supporting Information Part 2, one can see that the free energy results also reveal that A-path 2 is more favorable than other pathways. Due to the contributions of the entropy, the free energies are all higher than the total free energies of the separate reactants.

3.1.2. Water-Assisted Hydrolysis Reaction of PFA. In this section, the water-assisted hydrolysis mechanism with the three pathways (B-path 1, B-path 2, and B-path 3) is clarified. In these pathways, one water molecule serves as a bridge to help the transfer of the hydrogen atom in the hydrolysis reaction. On the PES of the water-assisted hydrolysis reaction of PFA, four different transition states were also located and their optimized structures are depicted in Figure 3. The optimized Cartesian coordinates and geometrical structures of all stationary points along the PES are also shown in Supporting Information Part 1 and Part 2, respectively.

B-Path 1. As shown in Figure s5, the geometries of complexes TP1−CM1 and TP1−CM2, transition states TP1−TS1 and TP1−TS2, and the intermediate TP1−IM were optimized at the B3LYP/6-31G(d,p) level. In TP1−CM1, the distances of Hw1−O1, Hw3−Ow1, Ow2−H1, and Hw4-N2 are 1.9633, 1.9366, 2.0871, and 2.8210 Å, respectively. TP1−TS1 is a six-membered ring transition state. The distances of Hw1−O1, Hw1−Ow1, Hw3−Ow1, Hw3−Ow2, Ow2−C1, and Hw4-N2 are 1.3670, 1.1046, 1.2764, 1.1589, 1.5420, and 1.6723 Å, respectively. The imaginary frequency is 1074.04i cm^{-1}. IRC results show that this step is associated with the coupling of the transfer of Hw3 atom from Ow2 to Ow1 atoms and the transfer of Hw1 atom from Ow1 to O1 atoms. And then, the intermediate was also offered after the reaction overcame the transition state TP1−TS1. In TP1−TS1, it is also a tetrahedral geometry with two OH groups attached on the C1 atom. The distances of Hw4-N2, Ow2−C1, and C1−N1 are 1.8751, 1.4016, and 1.4918 Å, respectively. Although the distance of Hw4−N2 is 1.8751 Å in TP1−IM, which is 0.2028 Å longer than that in TP1−TS1, it is also indicated that the Hw4 atom can transfer from Ow2 to N2 atoms due the short distance. Therefore, the transition state TP1−TS2 was located in our calculations. In TP1−TS2, the distances of Hw4−N2, Hw4-Ow2, and C1−N1 are 1.1363, 1.4042, and 1.6451 Å, respectively. The imaginary frequency is 661.13i cm^{-1}, which is also associated with the coupling of the transfer of Hw4 atom and the C1−N1 bond stretch mode, same to the transition state OP1−TS2. In TP1−CM2, the distances of Hw4−Ow2 and H1−N2 are 1.9156 and 2.3427 Å. It is turned out that, compared with the second step in A-path 1, the intermediate TP1−IM, transition state TP1−TS2, and the complex TP1−CM2 in the second step in B-path 1 are very close to OP1−IM, OP1−TS2, and OP1−CM2, respectively.

B-Path 2. As presented in Figure s6, the complexes TP2−CM1 and TP2−CM2 and the transition state TP2−TS were also optimized at the B3LYP/6-31G** level. In TP2−CM1, the distances of Hw4-O2, Hw4-N2, Hw2−Ow2, and H1−Ow1 are 1.8200, 2.8421, 1.800, and 2.0674 Å, respectively. TP2−TS is an eight-membered ring transition state, in which the distances of Hw4−N2, Hw4−Ow2, Hw2−Ow2, Hw2−Ow1, Ow1−C1, and C1−N1 are 1.3470, 1.1517, 1.1468, 1.2675, 1.6336, and 1.5993 Å, respectively. The imaginary frequency is 977.09i cm^{-1}. IRC results show that this step is associated with the coupling of the transfer of Hw2 atom from Ow1 to Ow2 atoms, the transfer of Hw4 atom from Ow2 to N2 atoms, and the addition of Ow1 to C1 atoms, leading to the cleavage of the C1−N1 bond. In TP2−CM2, the distances of Hw4-Ow2, Hw3−

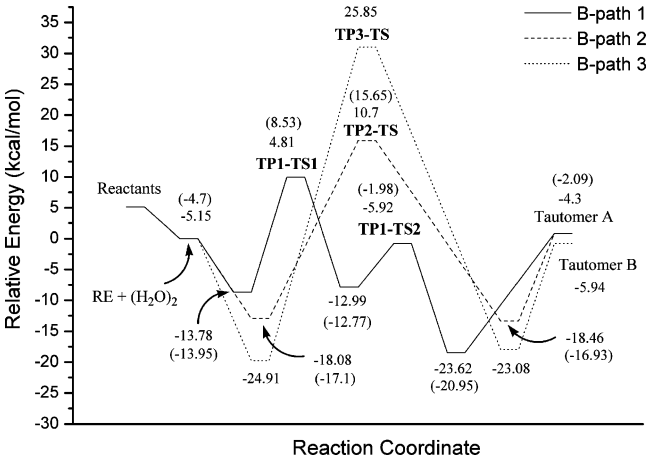

Figure 4. Energies profiles in water-assistant hydrolysis of PFA.

O2, Hw2−Ow1, and H1−N2 are 1.8451, 2.1025, 2.9480, and 2.3223 Å, respectively.

B-Path 3. For B-path 3, the reactant complex TP3−CM1, the transition state TP3−TS, and the product complex TP3−CM2 were located at the B3LYP/6-31G** level and their optimized geometries were given in Figure s7. In TP2−CM1, the distances of Ow2−H2, Hw3−Ow1, and Hw1−O1 are 1.7905, 1.7207, and 1.7970 Å, respectively. From Figure 1, one can see that the TP3−TS is also a six-membered ring transition state. The distances of Hw4−N1, Hw4−Ow2, Hw2−Ow2, Hw2−Ow1, Ow1−C1, and C1−N1 are 1.3865, 1.1343, 1.1825, 1.2365, 1.6263, and 1.7857 Å, respectively. The imaginary frequency is 1153.05i cm^{-1}. The dihedral angle N1−C2−N1−C1 is −57.99°, which also indicates that the C1 atom is deviated from the plane of pyrimidine ring. IRC results show that this step is associated with the coupling of the transfer of Hw2 atom from Ow1 to Ow2 atoms, the transfer of Hw4 atom from Ow2 to N1 atoms, and the addition of Ow1 to C1 atoms, leading to the cleavage of the C1−N1 bond. In TP3−CM2, the distances of Hw4−Ow2, Hw3−N1, Hw2−Ow1, and H1−O2 are 1.8984, 1.9886, 2.1672, and 2.2510 Å, respectively.

In addition, those stationary points on the PES of the water-assisted hydrolysis reaction were also optimized at the MP2/6-31G** level. The corresponding structures parameters are also presented in Figures s5 and s6. It is found that the structures located at the MP2/6-31G** level are very close to these located at the B3LYP/6-31G** level, except the complex TP2−CM1. In B-path 2, the other reactant complex TP2−CM3, which is different from the complex TP2−CM1, was obtained at the MP2/6-31G** level and also shown in Figure s6. In TP2−CM3, the distances of Hw4-N2, Ow2−Hw2, Ow1−C1, and Ow1−N1 are 2.0129, 1.8880, 2.8757, and 3.1524 Å, respectively. The dihedral angle Ow1−C1−N1−*C2* is 55.4°, implying that one water molecule is above the PFA plane and near to the C1 atom.

The electronic energy and free energy profiles for three pathways in the water-assisted hydrolysis in the gas phase are shown in Figure 4 and Figure s8 of Supporting Information Part 2. Table 2 lists the relative energies and free energies to reactant complex. Note that the energy values were also added with corresponding ZPVEs and thermal corrections. From Table 2 and Figure 4, one can see that B-path 1 is most favorable in three pathways, which is different from the results in the direct hydrolysis reaction. For B-path 1, one can see that the rate-limiting step is to surmount the transition state TP1−TS1. The energy barrier of the rate-limiting step is 18.59 kcal/mol at the B3LYP/6-31G** level in vacuum, while it increases to 22.48 kcal/mol at the MP2/ 6-31G** level in vacuum. For B-path 2, the energy barrier is 28.78 and 32.75 kcal/ mol in vacuum at the B3LYP/6-31G** and MP2/6-31G** levels, respectively. For B-path 3, there is a high barrier of 50.76 kcal/mol in vacuum at the B3LYP/6-31G** level, indicating that B-path 3 is difficult to undergo in the PFA hydrolysis reaction. Therefore, the re-optimizations of the stationary points at the MP2/6-31G** level were not carried out for B-path 3 in our work.

TABLE 2: Relative Energies, Free Energies, and Solvation Energies to Reactant Complex in Water-Assisted Hydrolysis of PFA (in kcal/mol)

	B3LYP/6-31G(d,p)		MP2/6-31G(d,p)		Monte Carlo
	ΔE(gas)	ΔG(gas)	ΔE(gas)	ΔG(gas)	$\Delta(\Delta G$(sol))
			B-path 1		
TP1−CM1	0.0	0.0	0.0	0.0	0.0
TP1−TS1	18.59	24.14	22.48	27.85	−2.52
TP1−IM	0.79	4.57	1.18	4.67	1.34
TP1−TS2	7.86	12.0	11.97	15.59	−1.19
TP1−CM2	−9.84	−9.15	−7.0	−7.11	−2.55
			B-path 2		
TP2−CM1	0.0	0.0	0.0	0.0	0.0
TP2−TS	28.78	32.75	32.75	37.06	−0.46
TP2−CM2	−0.38	−0.93	0.17	−0.26	6.71
			B-path 3		
TP3−CM1	0.0	0.0	−	−	−
TP3−TS	50.76	52.98	−	−	−
TP3−CM2	1.83	−0.37	−	−	−

3.2. Solvent Effects Determined by Monte Carlo Simulations. As stated above, due to the high-energy barrier, the solvent effect on B-path 3 was not taken into account in this study. So only five pathways, A-path 1, A-path 2, A-path 3, B-path 1, and B-path 2, of the hydrolysis reactions of PFA were studied in water using the free energy perturbation method implemented in BOSS 4.2 program.[34] The changes in free energies of solvation for the activation and reaction procedures of the direct and the water-assisted hydrolysis reactions are also listed in Table 1 and 2, respectively. Figure 5 depicts the relative potential energy profiles $E_{MEP}(s)$ of five reaction paths along the minimum energy path (MEP) in the gas phase and in water. From Figure 5, it is found that the solvent effect can slightly decrease the energy barrier in each pathway. That is to say, the solvent water can help and accelerate the PFA hydrolysis reaction in bulk water. From Tables 1 and 2, it is found that the differences in the free energies of solvation between OP2−CM1 and OP2−TS of A-path 2 and between TP1−CM1 and TP1−TS1 of B-path 1 are −4.29 and −2.52 kcal/mol, respectively. For an aqueous solution, the free energies of activation of the rate-limiting steps of five pathways were calculated by combining B3LYP/6-31G(d,p) calculation with Monte Carlo simulation and increase in the following order: B-path 1(21.62 kcal/mol) < A-path 2 (23.37 kcal/mol) < B-path 2 (32.29 kcal/mol) < A-path 1 (40.92 kcal/mol) < A-path 3 (45.83 kcal/mol). It is clear that both pathways, B-path 1 and A-path 2, have the high possibility to occur in the PFA hydrolysis reaction. However, B-path 1 is slightly more favorable than A-path 2. From Figure 5, one can see that the transition states of the second step in both A-path 1 and B-path 1 shift slightly in water, resulting in the elongating of the C1−N1 bond length. Near the complex OP2−CM1, a shallow potential well also exists in water, which corresponds to the complex OP2−CM3 located at the MP2/6-31G** level.

The solute−water energy pair distributions (EPD) of A-path 2 and B-path 1 were plotted in Figures 6 and 7, respectively. The plots give the number of solvent molecules on the *y*-axis that interact with the solute with the interaction energy shown on the *x*-axis. The bands at low-energy result from the hydrogen-

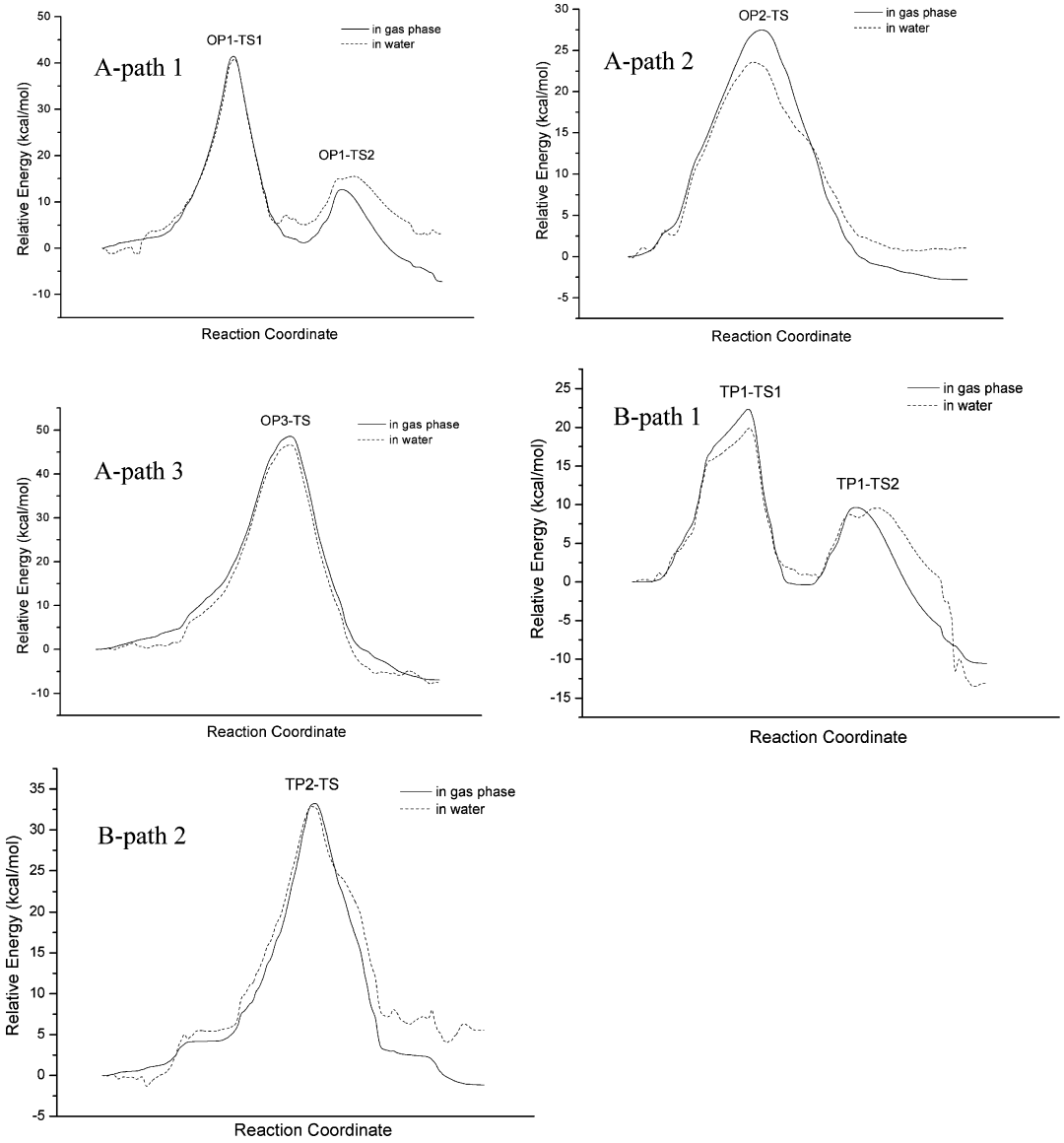

Figure 5. Potential energy profiles of five pathways in gas phase and water for PFA hydrolysis reaction.

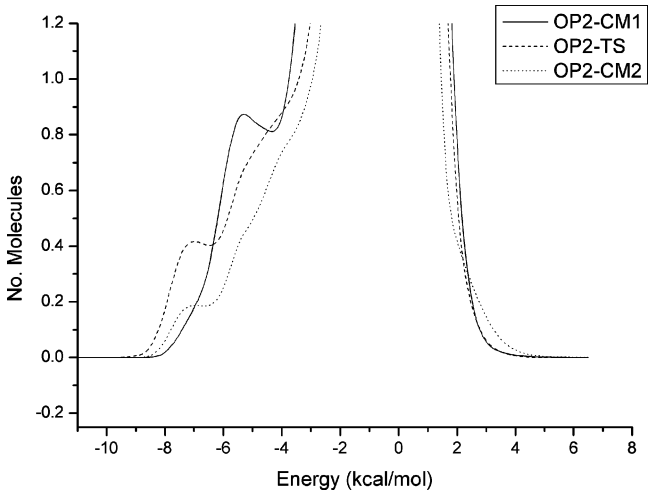

Figure 6. Pair-energy distributions of the solute-water interaction for OP2−CM1, OP2−TS, and OP2−CM2 in water in A-path 2.

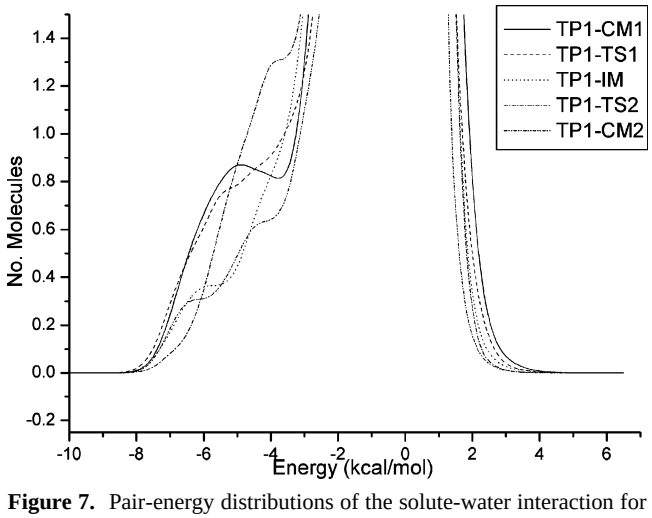

Figure 7. Pair-energy distributions of the solute-water interaction for TP1−CM1, TP1−TS, TP1−IM, TP1−TS2, and TP1−CM2 in water in B-path 1.

bonded solvent molecules and the spike centered at 0 kcal/mol comes from the weak interactions between the solute and many distant solvent molecules in outer shells. For A-path 2, from Figure 6, hydrogen bonding in water is reflected in the left-most region with energies more attractive than ca. −4.0 kcal/mol. The hydrogen-bonded energy band for OP2−CM1 in water covers the range from −9.0 to −4.0 kcal/mol. Integration of the bands from −9.0 to −4.0 kcal/mol yields 4.56, 4.90, and

3.08 water molecules for OP2−CM1, OP2−TS, and OP2−CM2, respectively. It is implied that the solvent effect on the transition state OP2−TS is slightly stronger than that on the complex OP2−CM1, lowering the energy barrier of A-path 2 in bulk water. For B-path 1, as presented in Figure 7, one can see that the hydrogen-bonded energy band for TP1−CM1 in water ranges from −9.0 to −3.5 kcal/mol. Integration of the bands from −9.0 to −3.5 kcal/ mol forms 5.60, 5.78, 4.15, 5.80, and 3.65 water molecules for TP1−CM1, TP1−TS1, TP1−IM, TP1−TS2, and TP1−CM2, respectively. This indicates that the solvent effect of water on the transition state TP1−TS1 is also slightly stronger than that on the complex TP1−CM1, resulting in the decrease of the energy barrier in the first step of B-path 1 in bulk water.

4. Conclusion

In this article, the mechanism of the PFA hydrolysis reaction was studied with the B3LYP/6-31G(d,p) and MP2/6-31G(d,p) methods. Two types of reaction processes were taken into account in our calculations. One is a direct hydrolysis mechanism, including one water molecule in the hydrolysis reaction; the other is a water-assisted hydrolysis process with two water molecules. For each reaction mechanism, three pathways were explored. Furthermore, solvent effects of water on three pathways in direct hydrolysis and two paths in the water-assisted hydrolysis reaction were evaluated by MC-FEP method. In water, all transition states of PFA hydrolysis reaction were stabilized by solvation. Our results indicated that, out of the six investigated pathways, the following two have the highest possibility to occur: namely, a water-assisted stepwise reaction path (B-path 1) and a direct concerted reaction path (A-path 2). Moreover, B-path 1 can proceed slightly more favorably than A-path 2 both in the gas phase and bulk water. The mechanisms are different from those of formamide hydrolysis[16] due to the neighboring group effect of the nitrogen atom of the pyrimidine ring.

Acknowledgment. This project has been supported by the National Natural Science Foundation of China (Grant Nos. 20473055 and 20533060) and the Teaching and Research Award Program for Outstanding Young Teachers in Higher Education Institutions of MOE, China.

Supporting Information Available: The optimized Cartesian coordinates and geometrical structures of all stationary points along the PES are shown in Supporting Information Part 1 and Part 2, respectively. This material is available free of charge via the Internet at http:// pubs.acs.org.

References and Notes

(1) Kobayashi, R. *J. Phys. Chem.* **1998**, *102*, 10813.
(2) Podolyan, Y.; Rubin, Y. V.; Leszczynski, J. *Int. J. Quant. Chem.* **2001**, *83*, 203.
(3) Fogarasi, G. *J. Phys. Chem. A* **2002**, *106*, 1381.
(4) Gould, I. R.; Green, D. V. S.; Young, P.; Hillier, I. H. *J. Org. Chem.* **1992**, *57*, 4434.
(5) Sobolewski, A. L.; Adamowicz, L. *J. Chem. Phys.* **1995**, *102*, 5708.
(6) Broo, A.; Holmén, A. *J. Phys. Chem. A* **1997**, *101*, 3589.
(7) Aleman, C. *Chem. Phys. Lett.* **1999**, *302*, 461.
(8) Brown, R. D.; Godfrey, P. D.; McNaughton, D.; Pierlot, A. P. *J. Am. Chem. Soc.* **1989**, *111*, 2308.
(9) Kwiatkowski, J. S.; Bartlett, R. J.; Person, W. B. *J. Am. Chem. Soc.* **1988**, *110*, 2353.
(10) Stewart, E. L.; Foley, C. K.; Allinger, N. L.; Bowen, J. P. *J. Am. Chem. Soc.* **1994**, *116*, 129.
(11) Colominas, C.; Luque, F. J.; Orozco, M. *J. Am. Chem. Soc.* **1996**, *118*, 6811.
(12) Bodor, N.; Kaminski, J. J. *Annu. Rep. Med. Chem.* **1987**, *22*, 303.
(13) Gosselin, G.; Bergogne, M. C.; de Rutger, J.; de Clecq, E.;. Imbach, J. L. *J. Med. Chem.* **1986**, *29*, 203.
(14) Webb, T. R.; Mitsuya, H.; Broder, S. *J. Med. Chem.* **1988**, *31*, 1475.
(15) Anastasi, C.; Hantz, O.; Clercq, F. D.; Pannecouque, C. *J. Med. Chem.* **2004**, *47*, 1183.
(16) Kallies, B.; Mitzner, R. *J. Mol. Model* **1998**, *4*, 183.
(17) Cascella, M.; Raugei, S.; Carloni, P. *J. Phys. Chem. B* **2004**, *108*, 369.
(18) Xue, Y.; Kim, C. K. *J. Phys. Chem. A* **2003**, *107*, 7945−7951.
(19) Zhang, H.; Xue, Y.; Xie, D. Q.; Yan, G. S. *Acta Chim. Sinica* **2005**, *63*, 791.
(20) Xue, Y.; Zhang, H.; Xie, D. Q.; Yan, G. S. *Chem. J. Chin. U.* **2005**, *26*, 907.
(21) Xue, Y.; Kim, C. K.; Guo, Y.; Xie, D. Q.; Yan, G. S. *J. Comput. Chem.* **2005**, *26*, 994.
(22) Becke, A. D. *J. Chem. Phys.* **1993**, *98*, 5648.
(23) Parr, R. G.; Yang, W. *Density-Functional Theory of Atoms and Molecules*; Oxford University Press: Oxford, 1989.
(24) Ditchfield, R.; Hehre, W. J.; Pople, J. A. *J. Chem. Phys.* **1971**, *54*, 724.
(25) Hehre, W. J.; Ditchfield, R.; Pople, J. A. *J. Chem. Phys.* **1972**, *56*, 2257.
(26) Hariharan, P. C.; Pople, J. A. *Mol. Phys.* **1974**, *27*, 209.
(27) Gordon, M. S. *Chem. Phys. Lett.* **1980**, *76*, 163.
(28) Hariharan, P. C.; Pople, J. A. *Theo. Chim. Acta.* **1973**, *28*, 213.
(29) Fukui, K. *J. Phys. Chem.* **1970**, *74*, 4161.
(30) Breneman, C. M.; Wiberg, K. B. *J. Comput. Chem.* **1990**, *11*, 361.
(31) Frisch, M. J.; Trucks, G. W.; Schlegel, H. B.; Scuseria, G. E.; Robb, M. A.; Cheeseman, J. R.; Zakrzewski, V. G.; Montgomery, J. A.; Jr.; Stratmann, R. E.; Burant, J. C.; Dapprich, S.; Millam, J. M.; Daniels, A. D.; Kudin, K. N.; Strain, M. C.; Farkas, O.; Tomasi, J.; Barone, V.; Cossi, M.; Cammi, R.; Mennucci, B.; Pomelli, C.; Adamo, C.; Clifford, S.; Ochterski, J.; Petersson, G. A.; Ayala, P. Y.; Cui, Q.; Morokuma, K.; Malick, D. K.; Rabuck, A. D.; Raghavachari, K.; Foresman, J. B.; Cioslowski, J.; Ortiz, J. V.; Stefanov, B. B.; Liu, G.; Liashenko, A.; Piskorz, P.; Komaromi, I.; Gomperts, R.; Martin, R. L.; Fox, D. J.; Keith, T.; Al-Laham, M. A.; Peng, C. Y.; Nanayakkara, A.; Gonzalez, C.; Challacombe, M.; Gill, P. M. W.; Johnson, B.; Chen, W.; Wong, M. W.; Andres, J. L.; Gonzalez, C.; Head-Gordon, M.; Replogle, E. S.; Pople, J. A. *Gaussian 03*, Revision D. 01; Gaussian, Inc.: Pittsburgh PA, 2005.
(32) Jorgensen, W. J.; Ravimohan, C. *J. Chem. Phys.* **1985**, *83*, 3050.
(33) Zwanzig, R. W. *J. Chem. Phys.* **1954**, *22*, 1420.
(34) Jorgensen, W. J. *BOSS*, Version 4.2: Yale University: New Haven, CT, 2000.
(35) Duffy, E. M.; Severance, D. L.; Jorgensen, W. J. *J. Am. Chem. Soc.* **1992**, *114*, 7535.
(36) Kaminski, G. A.; Jorgensen, W. J. *J. Phys. Chem. B* **1998**, *102*, 1787.
(37) Jorgensen, W. J. *J. Phys. Chem.* **1986**, *90*, 1276.
(38) Jorgensen, W. J.; Chandrasekhar, J.; Madura, J. D.; Impey, R. W.; Kelin, M. L. *J. Chem. Phys.* **1983**, *79*, 926.